

On the connection between wavelet variance and spectral statistics of SAR backscatter random processes

Lecture Notes

Gianfranco De Grandi (University of Aberystwyth)

Edward Mitchard (University of Edinburgh)

Relevance of two-point statistics in connection with SAR imagery textural characterization, in particular of the Fourier spectral analysis and the autocorrelation function (ACF), was pointed out in a seminal work published in the late 80s [1]. This work was targeted to supervised classification, where textural class parameters were estimated from SAR spatial statistics. Analysis was carried out based on stationary Rayleigh statistics for the envelope of the received field, and under the condition of a delta correlated fading component. In this framework, a method was derived for the estimation of the underlying radar cross section ACF from experimental data, whilst no specific model for the surface fluctuations was proposed. This line of research was extended by a theoretical model for non-Rayleigh SAR scattering statistics, covering the case of correlations between scatterers in the resolution cell (or fluctuating cross section), and finite illumination window [2][3]. The surface fluctuations were described by a Gamma distribution and a Lorentzian spectrum (exponential ACF). This model is particularly relevant when imaging forest at the high resolution (order of 1 to 3 meters) afforded by some of currently deployed space-borne SAR instruments. These contributions were the springboard over which interest in space-frequency analysis of SAR backscatter took momentum [4][5][6][7].

Wavelet frame spatial statistical measures are rooted in the groundwork established by the classical Fourier ACF analysis adopted in those research works, but extend it in several respects: by enabling space-scale analysis (through good localization in the space-frequency domain); by the capability of dealing with non-stationary processes; providing statistically better and computationally more efficient estimators. The reader is referred to [8] for a discussion on this topic. It appears therefore interesting to establish, for those random processes described by the models mentioned above, the connection between the wavelet space-scale statistics (wavelet variance and covariance) and the ACF based characterization.

For the purpose, analytical and numerical derivations were undertaken to illustrate the response of the wavelet scaling signatures to given correlation properties of the input spatial random field (SRF), including those assumed in the models in [2].

Analysis is carried out in the continuous scale-space assuming a signal representation provided by a wavelet frame basis defined in [16]. The wavelet is the first derivative of a box spline of order 3, with Fourier transform:

$$\widehat{w}(\omega) = -i \frac{\omega}{4} \left(\frac{\sin(\frac{\omega}{4})}{\frac{\omega}{4}} \right)^4 e^{-i\frac{\omega}{2}} \quad (1)$$

The wavelet transform is:

$$W_f(s, b)|_{1/2} = s^{-\frac{1}{2}} \int_{-\infty}^{+\infty} f(x) w\left(\frac{x-b}{s}\right) db \quad (2)$$

The normalization $s^{-1/2}$ preserves the L^2 norms of the dilated wavelets.

The wavelet variance is:

$$\langle W_f^2 \rangle(s) = \int_{\varepsilon} [W_f(s, b)]^2 db \quad (3)$$

Where ε is the estimation interval. When computed globally over the whole signal the wavelet variance (3) is equivalent to the energy spectrum $E_f(k)$ provided by the Fourier transform.

The wavelet operator is linear. Since the transform (2) is a convolution of the signal with the mother wavelet dilated by s , in the Fourier domain the transform at scale s is equivalent to:

$$\widehat{W}_f = s^{-1/2} \widehat{w}_s(\omega) \mathfrak{F}_f(\omega) \quad (4)$$

Where $\widehat{w}_s(\omega) = s\widehat{w}(s\omega)$ is the Fourier transform of the dilated wavelet at scale s , with $\widehat{w}(\omega)$ given in (1), and \mathfrak{F}_f is the Fourier transform of the signal.

Given an input noise process with known spectral properties, the spectrum of the signal at the output of a linear system whose transfer function is given by the wavelet Fourier spectrum is [14]:

$$S_{V_s}(\omega) = |s^{-1/2} \widehat{w}_s(\omega)|^2 S_f(\omega) \quad (5)$$

Where S_f is the spectrum of signal f .

The wavelet variance (3) can be finally computed from the ACF of the output signal at lag 0:

$$\langle w(s)^2 \rangle = \mathcal{R}(\tau = 0) = \mathfrak{F}^{-1}(S(\omega, s))|_{\tau=0} = \frac{1}{2\pi} \int S(\omega, s) d\omega \quad (6)$$

Where $S(\omega) = \widehat{W}_f \widehat{W}_f^*$, and $\mathcal{R}(\tau)$ is the ACF of the stationary process.

Regarding the wavelet co-variance, let us consider the wavelet transform of two signals W_X, W_Y .

The cross-spectrum of the transforms from (4) is:

$$\mathfrak{F}(W_X \otimes W_Y) = \mathfrak{F}(W_X) \mathfrak{F}(W_Y) = s^{-1} |\widehat{w}|_s^2 \mathfrak{F}_X(X) \mathfrak{F}_Y(Y) = s^{-1} |\widehat{w}|_s^2 \mathfrak{F}(X \otimes Y) \quad (8)$$

Therefore the cross-correlation function (CCF) of the wavelet transform is linked to the cross-correlation of the input signals through the dilated wavelet frequency response. Finally the wavelet covariance is computed from the CCF at lag 0:

$$\langle w_X w_Y \rangle(s) = \mathfrak{F}^{-1}_{\tau=0} \left(s^{-1} |\widehat{w}|_s^2 \mathfrak{F}_X(X) \mathfrak{F}_Y(Y) \right) \quad (9)$$

These results will be used next to derive the wavelet variance response in a number of test cases consisting of input random processes with different correlation properties.

- 1) White noise (e.g. delta correlated speckle statistics with constant radar reflectivity)

$$\mathcal{R}(\tau) = \langle I \rangle^2 \delta(\tau) \quad (10)$$

$$\Gamma(\omega) = \langle I \rangle^2 \quad (11)$$

$$\langle w(s)^2 \rangle = \frac{2 \langle I \rangle^2}{3} \quad (12)$$

The wavelet variance is scale independent.

2) 1/f process(e.g. fractal surface [9][10][11])

$$S(\omega) = \frac{\sigma^2}{|\omega|^\beta} \quad (13)$$

$$\frac{1}{\pi} \left(\langle I \rangle^2 |\tau|^{\beta-1} \Gamma(1-\beta) \sin \frac{\pi\beta}{2} \right) \quad (14)$$

$$\langle w(s)^2 \rangle = \text{const} \langle I \rangle^2 s^2 \text{ for } \beta = 2 \quad (15)$$

The dependence of the wavelet variance with scale is linear in log-log scale, with the first derivative proportional to the spectral exponent.

3) Correlated surface (Gamma distributed RCS) with exponential ACF (Lorentzian spectrum)

[2]

$$\mathcal{R}(\tau) = \langle I \rangle^2 + \frac{\langle I \rangle^2}{\nu} e^{-\beta|\tau|} \quad (16)$$

Where $\langle I \rangle$ is the mean scattered intensity, ν is the order parameter of the Gamma distribution, β is the inverse correlation length.

$$S(\omega) = \frac{\langle I^2 \rangle \beta}{\beta^2 + \omega^2} + 2\pi \langle I \rangle^2 \delta(\omega) \quad (17)$$

Where $\delta(x)$ is the Dirac distribution.

The integral (6) (wavelet variance) was evaluated numerically as a function of scale and for parameters $\nu = 0.375$ and $\beta = 0.1, 0.4, 0.8$. The resulting curves are shown in the log-log graph in Fig.1.

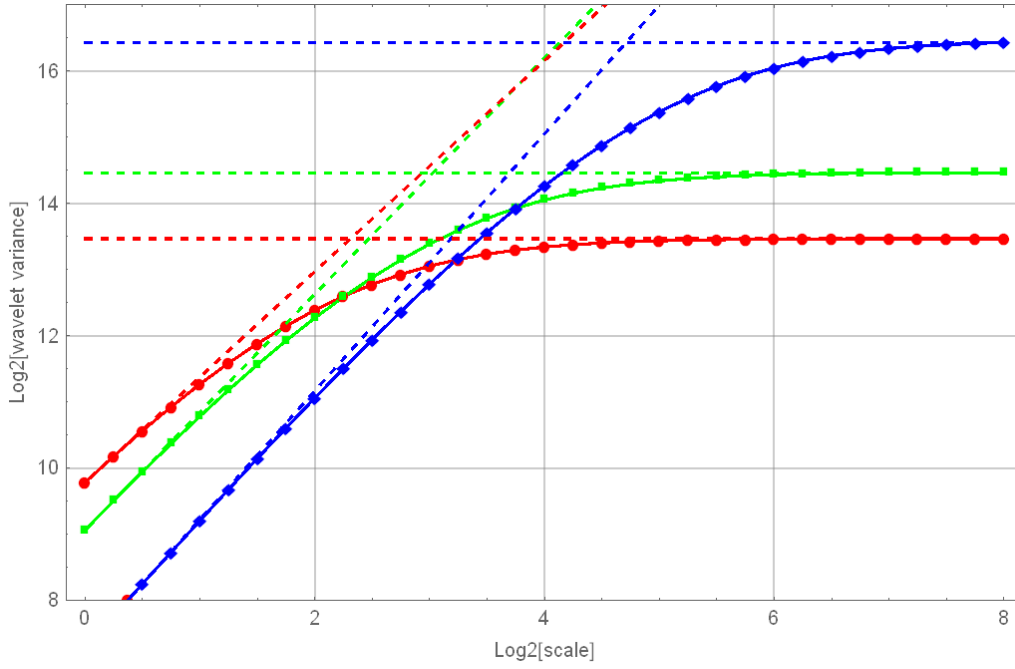


Fig. 1 Graph of the wavelet variance for a Gamma distributed RCS with exponential ACF. The input random process model was parametrized with inverse correlation length $\beta = 0.1, 0.4, 0.8$ and order parameter $\nu = 0.375$. The signatures for the three cases are represented, respectively, by red, green and blue (circle, square and diamond symbols) solid lines. Dotted lines mark the tangent lines to $\langle w^2 \rangle$ at scale $s=1$, and the asymptotic values at large scales.

The red (circles), the green (squares) and the blue (diamond) solid lines correspond respectively to the inverse correlation length values $\beta = 0.1, 0.4, 0.8$. The dotted lines mark the tangent of the curve at scale $s=1$, and the asymptotic values of the wavelet variance.

Let us consider the derivative of the wavelet variance at scale $s=1$. The wavelet spectrum at scale s can be approximated by:

$$s \left| -\frac{1}{2} + \frac{1}{2} e^{-i s \omega} \right|^2 \quad (18)$$

The derivative of the wavelet variance at scale 1, this corresponding to $\Re(0)'$, can be derived from the derivative under the integral sign in (6). Retaining only first order terms in ω in the derivative of (18) :

$$\langle w(1)^2 \rangle' \simeq \frac{\langle I \rangle^2}{\nu} \tan^{-1} \frac{2\pi}{\beta} \quad (19)$$

For $\beta \leq 1$ the dependence of the signature slope at $s=1$ is linear in β and proportional to the signal intensity second moment. Therefore $\langle w(1)^2 \rangle'$ and $\langle w(1)^2 \rangle$ supply information on the RCS Γ distribution order parameter, and on the ACF inverse correlation length.

The asymptotic value of the wavelet variance can be derived by considering that at large scales the input signal becomes uncorrelated with spectrum $G(\omega) = \langle I^2 \rangle + \langle I \rangle^2$. The limit under the integral sign in (6) is:

$$\lim_{s \rightarrow \infty} \int \langle I \rangle^2 |s^{-1/2} \widehat{w}_s(\omega)|^2 d\omega = \frac{2}{3} \pi (\langle I^2 \rangle + \langle I \rangle^2) \quad (20)$$

Therefore the asymptotic value of the wavelet variance provides information on the first two moments of intensity.

4) Cross-correlation between two stationary processes with exponential ACFs

Numerical evaluation of integral (9) was performed assuming the two stationary input processes being characterized by exponential ACFs, and an exponential CCF, with given parameters.

Moreover, the Schwartz inequality condition is imposed on the second moments of intensity:

$$|\langle I_1 I_2 \rangle|^2 \leq \langle I_1^2 \rangle \langle I_2^2 \rangle \quad (21)$$

The resulting wavelet co-variance was also normalized by the wavelet variance.

Test cases are considered with processes with equal backscatter intensity and order parameters, and ACFs and CCF with different inverse correlation lengths, these being:

$$\beta_1 \beta_2 = (0.8, 0.1) \quad (0.4, 0.1) \quad (0.1, 0.1) \quad \gamma = (0.5, 0.2, 0.1)$$

Where $\beta_1 \beta_2$ are the inverse correlation lengths of the ACFs and γ is the inverse correlation length of the CCF.

Results are reported in Fig. 2, with the red, green and blue lines corresponding to the cases listed above. Notice that the normalized wavelet variance depends both on the CCF between the two processes (through integral (9)), and on the ACFs of each process, these being reflected in the normalizing variances in the denominator. Longer CCF correlation length tends to flatten the scaling dependence of the wavelet covariance (see blue line). With shorter CCF correlation length,

the dependence on the ACFs weighs in; the wavelet covariance decreases more rapidly with scale (i.e. decorrelates more) as a function of the difference between the ACFs correlation lengths. In other words, the wavelet covariance provides, in this case, a measure of the textural diversity between the two processes.

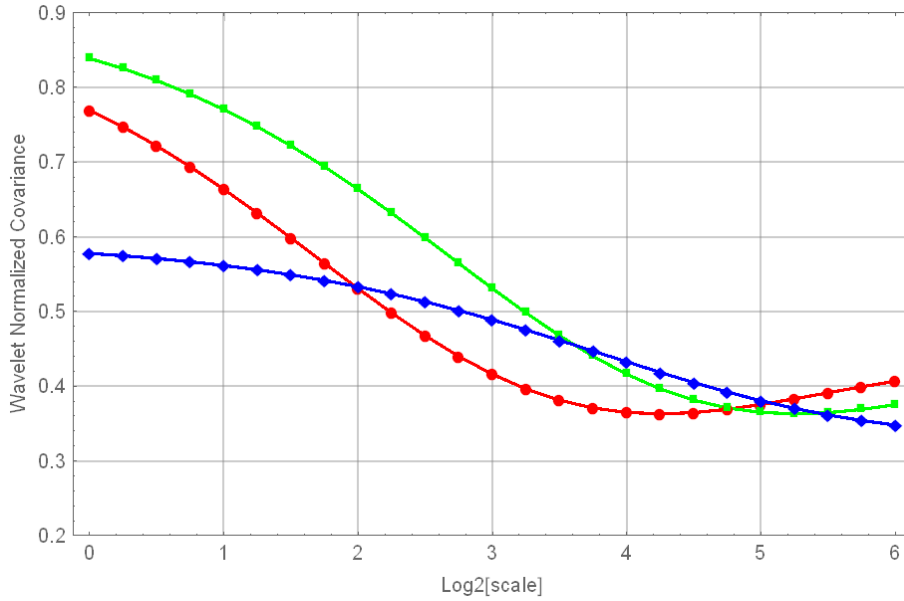


Fig. 2 Normalized wavelet co-variance as a function of scale. Three cases were analyzed. Parameters of input processes' model were: $\beta_1\beta_2 = (0.8, 0.1) (0.4, 0.1) (0.1, 0.1)$ for the ACFs inverse correlation lengths, and $\gamma = (0.5, 0.2, 0.1)$ for the CCF inverse correlation length. The three cases correspond to the red, green and blue lines (circle, square, diamond symbols).

5) Effects due to coherent imaging and illumination beam size

In the previous analysis the connection was established between the wavelet variance scaling and the correlation properties of the illuminated surface (i.e. the RCS). In other words, we have assumed a situation where perfect reconstruction of RCS had been somehow accomplished before estimating the wavelet statistics. We consider now the case where the coherent interaction of the scattering elements and the illumination beam finite size are included in the model of the backscattered intensity ACF, as it was proposed in the correlated K-distributed model in [12], [13 (3.8)]:

$$\mathcal{R}(\tau) = \langle I \rangle^2 + \langle I \rangle^2 e^{-\frac{\tau^2}{\sigma^2}} + \frac{\langle I \rangle^2}{v} \left(e^{-\beta\tau^2} \otimes \left| e^{-\frac{\tau^2}{\sigma^2}} \right|^2 \right) \quad (22)$$

Where the illumination beam is assumed to have a Gaussian profile with σ being the 1/e width, ν is the order parameter of the K distribution, β is the inverse correlation length.

Numerical evaluation of the integral (6) using the intensity ACF (22) yields the wavelet variance signatures represented in Fig. 3. Parameters were: $2\sigma = 3$, $\nu = 0.375$ and $\beta = 0.01, 0.05, 0.1$, these corresponding to the blue (diamond), green (square) and red (circle) lines.

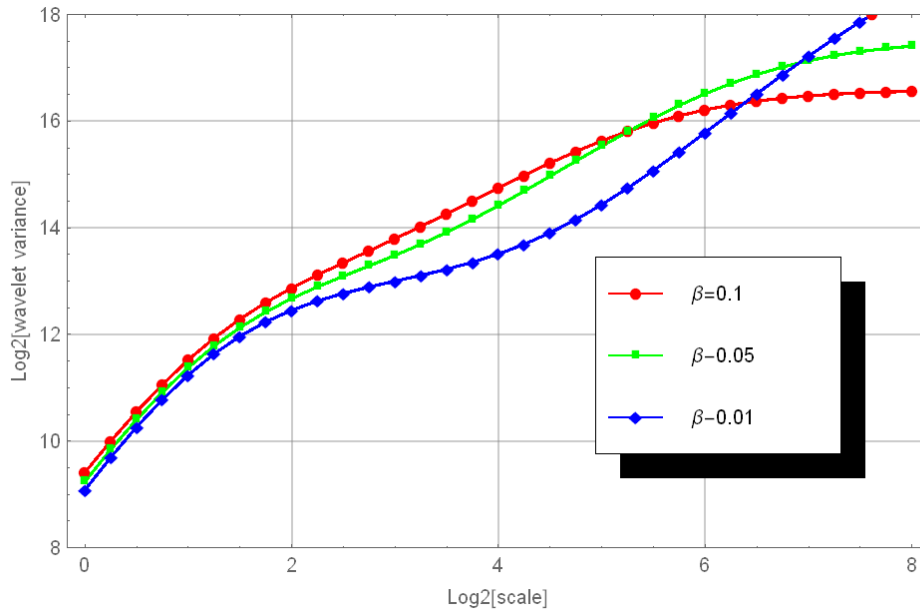


Fig. 3 Wavelet variance signatures for a K-distributed clutter model including effects due to the instrument point spread function (PSF). The red, green, blue curves (circle, square, diamond symbols) correspond to cases with model parameters of : $2\sigma = 3$, $\nu = 0.375$ and $\beta = 0.01, 0.05, 0.1$.

Information about the underlying RCS at short scales ($s=1,4$), i.e. within the instrument's resolution, is shadowed by the impulse response function of the instrument, and is therefore unobtainable. The RCS correlation length can still be estimated from the onset of the asymptotic value, but only within the region of scales outside the influence of the instrument PSF.

REFERENCES

- [1] F.T. Ulaby, F. Kouyate, B. Brisco and T.H. Williams, "Textural Information in SAR Images", IEEE Transactions on Geoscience and Remote Sensing, vol. GE-24, no. 2, pp. 235 - 245, March 1986.

- [2] C.J. Oliver, "A model for non-Rayleigh scattering statistics", *OPTICA ACTA*, vol. 31, no. 6, p. 701-722, 1984.
- [3] C.J. Oliver, "The Representation of Correlated Clutter Textures in Coherent Images", *Inverse Problems*, vol. 4, pp. 843 - 866, 1988.
- [4] D.R. Sheen, L.P. Johnston, "Statistical and spatial properties of forest clutter measured with polarimetric synthetic aperture radar (SAR)", *IEEE Transactions on [Geoscience and Remote Sensing](#)*, vol. 30, no. 3, pp. 578 - 588, May 1992.
- [5] L. Kurvonen, M.T. Hallikainen, "Textural information of multitemporal ERS-1 and JERS-1 SAR images with applications to land and forest type classification in Boreal zone", *IEEE Transactions on [Geoscience and Remote Sensing](#)*, vol. 37, no. 2, Part 1, pp. 680 - 689, March 1999.
- [6] M.J. Collins, Jin Huang, "Uncertainties in the estimation of ACF-based texture in synthetic aperture radar image data", *IEEE Transactions on [Geoscience and Remote Sensing](#)*, vol. 36, no. 3, pp. 940 - 949, May 1998.
- [7] F. Bujor, E. Trouve, L. Valet, J.-M. Nicolas, J.-P. Rudant, "Application of log-cumulants to the detection of spatiotemporal discontinuities in multitemporal SAR images", *IEEE Transactions on Geoscience and Remote Sensing*, vol. 42, no. 10, pp. 2073 - 2084, Oct. 2004.
- [8] D.B. Percival, and A.T. Walden, "Wavelet methods for time series analysis", ch. 8.3, p. 306, Cambridge University press, 2000.
- [9] Stewart et al., "Brownian motion models for SAR imagery scene segmentation", *Proc. IEEE*, vol. 81, no. 10, October 1993.
- [10] Giorgio Franceschetti et al., "Scattering from Natural Rough Surfaces Modeled by Fractional Brownian Motion Two-Dimensional Processes", *IEEE Trans. On Antennas and Propagation*, vol. 47, no. 9, September 1999.
- [11] G.W. Wornell, "Wavelet-based representations for the 1/f family of fractal processes", *Proc. of the IEEE*, vol. 81, no. 10, October 1993.

- [12] C. J. Oliver, S. Quegan, *Understanding Synthetic Aperture Radar Images*, Chapter 5.21, Artech House, London, UK, 1998, ISBN 089006850X.
- [13] C. J. Oliver, "Correlated K-distributed clutter models", *Optica Acta: International Journal of Optics*, 32:12, 1515-1547.
- [14] B. Picinbono, "Random signals and systems", ch. 5.4, Prentice Hall International Editions, 1993.
- [15] G. De Grandi et al., "Target Detection and Texture Segmentation in Polarimetric SAR Images Using a Wavelet Frame: Theoretical Aspects", *IEEE Trans. GEO. REM. SENSING*, vol. 45, no. 11, November 2007.
- [16] S. Mallat, *A Wavelet Tour of Signal Processing*, London: Academic Press, 1998, ch. 5.5, pp. 152-154.